Raman and Electrochemical Probes of the Dissolution Kinetics of Tungsten in Hydrogen Peroxide

Gary S. Kanner*,† and Darryl P. Butt

Materials Science and Technology Division, MS G755, Los Alamos National Laboratory, Los Alamos, New Mexico 87545

Received: June 22, 1998

The interaction of tungsten with hydrogen peroxide was studied by Raman spectroscopy and electrochemical measurements. We found that W catalyzes the decomposition of peroxide into its ion, while the native oxide of W becomes increasingly hydrated and soluble. The decay of the peroxide concentration upon immersion of W is consistent with a model of 1-D diffusion to the W surface followed by a surface reaction with a heterogeneous rate constant of 3×10^{-5} cm/s. This model can also be used to explain the decrease of the H_2O_2 solution pH and the increase in open circuit potential of W that occurs while W is immersed in H_2O_2.

Introduction

There have been numerous studies on the Raman spectroscopy of tungsten oxides,[1−10] largely motivated by the need to understand the mechanisms of electrochromism in amorphous WO_3. The reaction governing this process is thought to be[11]

$$xH^+ + xe^- + WO_3 + zH_2O \rightarrow H_xWO_3 \cdot zH_2O \qquad (1)$$

Associated with this process is a change in the optical absorption that has been attributed to transitions due to either an intervalence charge transfer from W^{5+} to W^{6+} sites,[12] electrons that are trapped at oxygen vacancies or localized at tungsten ions,[13] or electrons localized on W^{6+} sites forming small polarons.[14] On a practical level, the ability to construct durable display devices from these compounds has been hampered by a lack of knowledge of the factors controlling the kinetics of coloration as well as the dissolution rate of WO_3 in acidic aqueous electrolytes. Using a combination of electrochemical techniques and infrared absorption, it has been found that both the electrochromic reaction and the rate of film dissolution increased as the porosity and water content of the films increased.[11]

More recently, tungsten has been considered for its potential as a neutron spallation source because of its high production and leakage rate of neutrons upon irradiation with high energy protons.[15] Any metal in this type of radiation environment or in nuclear reactors may be subject to corrosion by the very reactive species generated by the high energy particles in the surrounding cooling water.[16] One of the main contributors to corrosion in nuclear reactors is suspected to be hydrogen peroxide (H_2O_2),[17] which is primarily created by the combination of two OH radicals that are formed by radiolysis of the cooling water. This corrosive property of H_2O_2 actually makes it a popular etchant of Ti:W films.[18]

In this work, we studied tungsten immersed in a H_2O_2 solution in order to understand the nature of the interaction between a long-lived radiolysis product and a neutron spallation source. Specifically, we used Raman spectroscopy and electrochemical measurements to identify the nature of the native oxide of tungsten and to probe the reaction kinetics at the solid−solution interface. We model the kinetics with a one-dimensional diffusion equation for the migration of the peroxide molecules to a W surface with which they react. We find that this model gives reasonably good agreement with the measured dependence of the peroxide concentration, pH, and open circuit potential of tungsten on the time of immersion in H_2O_2. Consequently, this combination of structurally specific and electrochemical techniques provides a powerful method for characterizing interfacial reactions.

Experimental Section

Raman spectroscopy was performed using the 514.5 nm line from a Coherent Innova 100 Ar ion laser. Two different detection systems were used. In one, the scattered light was dispersed by a Spex 1817D Triplemate spectrometer and detected by a 298x1152 Princeton Instruments CCD. In the other, we used a 330x1100 Princeton Instruments CCD coupled to a 0.25-m Chromex spectrometer. Both CCDs were cooled by liquid nitrogen. Laser power at the sample was limited to 100 mW focused to a spot about 100 μm in diameter.

The sample consisted of a 1 mm thick 99.96% W (Alfa Aesar) 1/4 in. radius semicircular disk polished to a 1-μm finish and ultrasonically cleaned. The plate was immersed in a quartz cell with a 1×1 cm cross-section that was filled with 0.97 M hydrogen peroxide (Fisher ACS certified) to a level just barely above the uppermost surface of the W plate.

For the electrochemical measurements, the W plate was partially immersed in a fresh 0.97 M H_2O_2 solution, and the potential V was determined with respect to a $Hg/HgSO_4$ reference electrode using a voltmeter. The pH of this solution was measured using pH paper.

Results and Discussion

Raman Spectra. In recent studies using surface enhanced Raman spectroscopy (SERS),[19] we showed that the native tungsten oxide consists of a mixture of WO_3 and one of its hydrates. For our normal Raman studies of the effect of a long-lived radiolysis product on this oxide, we immersed (at time *t*

† Currently a visiting assistant professor at Department of Physics and Astronomy, Northern Arizona University, P.O. Box 6010, Flagstaff, AZ 86011-6010.

10.1021/jp982716a CCC: $15.00
Published on Web 10/30/1998

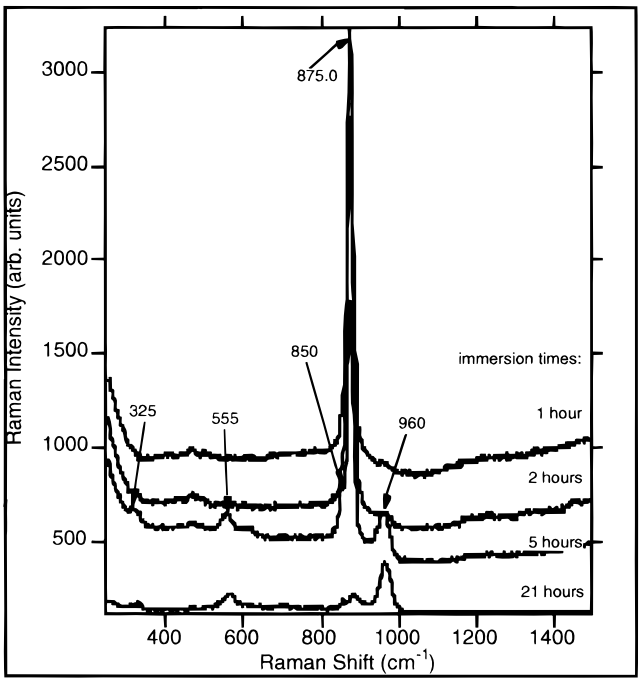

Figure 1. Raman spectra of the H_2O_2 solution surrounding a W plate as a function of immersion time.

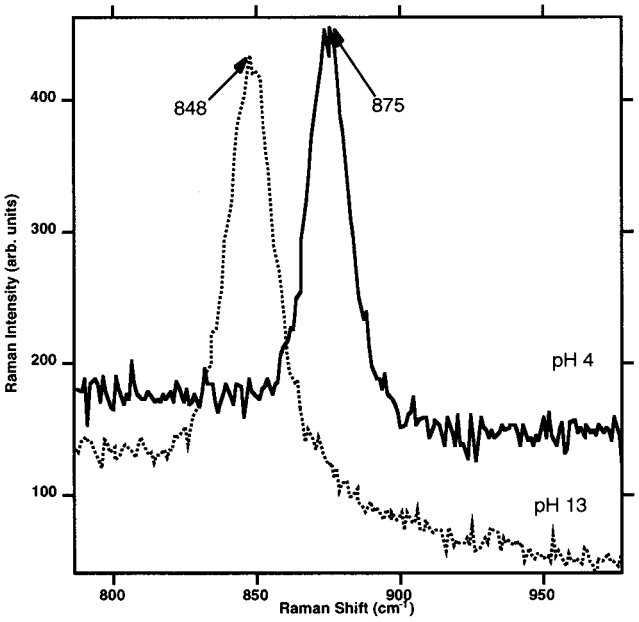

Figure 2. Raman spectra of hydrogen peroxide at pH 4 and pH 13.

$= 0$) a plate of unenhanced W in a solution of H_2O_2 and monitored the Raman spectrum of the surrounding solution (Figure 1) as a function of time. The spectrum of the peroxide solution for $t < 0$ is dominated by the O−O stretching mode of the H_2O_2 molecule at 875 cm^{-1}. Upon immersion of W in H_2O_2 (Figure 1), there is a gradual decrease of the O−O mode intensity accompanied by the formation of strong bands peaking around 325, 555, 849, and 960 cm^{-1}. None of these modes could be detected directly from the W surface but instead arose from the solution surrounding the W plate. One possible oxidation product of WO_3 is the soluble ion WO_4^{2-} according to

$$WO_3 + H_2O = WO_4^{2-} + 2H^+ \qquad (2)$$

The Raman spectrum of WO_4^{2-} consists of bands at 325, 835, and 933 cm^{-1};[3] only the lowest frequency mode (325 cm^{-1}) matches what we observe in Figure 1. In addition, we expect the concentration of WO_4^{2-} to be quite small for pH < 5, the upper limit in our measurement. As we show below, the pH of the solution becomes more acidic with time. Consequently, we rule out WO_4^{2-} as a product of the interaction between W and H_2O_2 at these pH levels. At acidic pH, the dominant species in solution is expected to be a protonated form of $W_{12}O_{42}^{12-}$, with Raman modes at 350, 420, 650, 900, 940, 965, and 980 cm^{-1}.[2] Instead, the Raman modes we observe more closely match those of hydrated tungsten trioxides. In particular, the bands at 325 and 960 cm^{-1} have been attributed to the stretching modes of W−OH_2 and W═O associated with the terminal bonds of hydrated tungsten oxide octahedra in the WO_3 crystal.[5]

Modes around 555 cm^{-1} have been assigned to a stretching vibration of W(O2) complexes.[6,21] A band at 560 cm^{-1} has also been observed as a Raman mode in aqueous tungstate solutions for 5.0 < pH < 7.4.[2] The frequency is also in the region of O−W−O bond deformations in the equatorial plane of hydrates.[5]

In addition to changes in intensity, the frequencies of the 550 and 960 cm^{-1} modes increase with immersion time τ. The frequency of the W═O stretch depends on the number z of water molecules in the unit cell of the crystalline tungsten trioxide $WO_3 \cdot zH_2O$. For example, for $z = 1/3$, 1, and 2, the frequencies are 945, 948, and 960 cm^{-1}, respectively.[5] In studies of the electrochromic reaction in acidic aqueous solution,[11] it was suggested that both the hydration and dissolution rates increase with the water content of the oxide film. Similarly, in the present experiments, we surmise that the degree of hydration z increases with τ; therefore, the W═O mode frequency increases with τ as well. Frequency increases of this mode have also been observed upon injection of protons and deuterons in $WO_3 \cdot 1/3H_2O$.[8] In our experiment, the blue shift may compete with a frequency decrease caused by electron transfer from the metal into antibonding orbitals of the adsorbed molecules.

The band at 850 cm^{-1} does not match the frequencies of tungsten oxide modes. However, it is close to the frequency of a mode attributed to the oxygen stretch of the peroxide ion HO^{2-}.[22] The ion is predicted to be the more stable form of peroxide for pH > 11.6.[20] Figure 2 shows the O−O stretching mode of peroxide at acidic and alkaline pH. At pH 4, the O−O mode is at 875 cm^{-1} but shifts to 848 cm^{-1} at pH 12.8. The presence of the ion in our measurements is surprising since, as we will show below, the pH of the solution was always less than 5. Nevertheless, we attribute the origin of this ion to the catalytic decomposition of H_2O_2 at the W surface according to

$$H_2O_2 = HO_2^- + H^+ \qquad (3)$$

The disappearance of the 850 cm^{-1} band after 20 h of immersion is, however, consistent with the instability of this ion at the low pH of our experiment.

Evaporation of the peroxide solution that had reacted with W yielded a yellow powder, similar in color to $WO_3 \cdot H_2O$.[20] However, the Raman spectrum of this powder (Figure 3) differed from that of $WO_3 \cdot H_2O$;[5] in addition to the W═O mode at 942 cm^{-1}, there is a strong band at 863 cm^{-1} and very little intensity in the region of the O−W−O deformation (645 cm^{-1}). The spectrum more closely matches that of crystalline polytungstates[1] and aqueous tungstate ions at low pH.[2] As shown in Figure 3, the Raman spectrum of the powder is similar to that of ammonium metatungstate ($(NH_4)_6H_2W_{12}O_{40} \cdot nH_2O$, $5 < n < 11$)

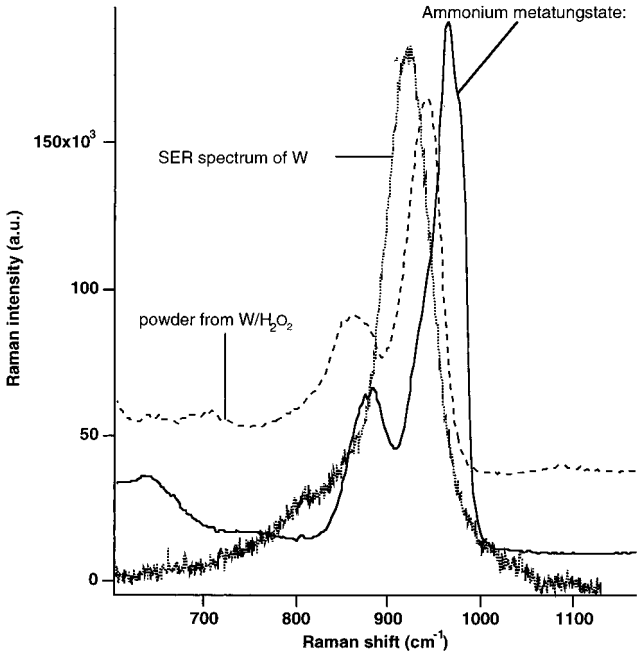

Figure 3. Raman spectrum of the powder formed upon evaporation of the solution in contact with the W plate as compared to the Raman spectra of ammonium metatungstate and the SER spectrum (ref 19) of W.

but is shifted downward by about 20 cm^{-1}. This similarity suggests that the interaction of H_2O_2 with W leads to the formation of a tungsten oxide hydrate with a coordination number slightly greater than 3.

The difference between the Raman spectrum of the oxide in solution (Figure 1) and that of the yellow powder (Figure 3) can be attributed to the different environments (water, air) surrounding the oxides, the resulting changes in bonding, and therefore, symmetry. The oxides in water and in air will almost certainly have different degrees of hydration. As has been shown, each hydrate has a unique crystal structure, leading to significant differences among their Raman spectra.[5]

In previous studies of etching of W electrodes by H_2O_2,[23] it was conjectured that a large portion of the native trioxide was transformed to WO_x, $2 < x < 3$. This oxide was preferentially removed when the electrode was rotated within the solution. As we have shown (ref 19) in SERS studies of W electrodes, however, the shape of the spectrum may primarily be a function of the ratio of the concentration in the oxide film of $WO_3 \cdot H_2O$ to that of WO_3. Therefore, we surmise that new oxide generated is a hydrated tungstate that is much more soluble than anhydrous WO_3. This explains why this oxide is selectively removed from the film when the solution is agitated.

The dynamics of the H_2O_2 Raman signal is shown in Figure 4. These data were determined from the relative Raman intensity of the O−O mode as a function of the W immersion time (Figure 1) and represent the decay of the peroxide molecules upon interaction with the W plate. In Figure 4, we also present the results of a model to compare with the measured temporal response; the details of this model will be discussed below.

Electrochemical Measurements. We gain further insight into the Raman spectra of Figure 1 by correlating them with the simplified Pourbaix diagrams (Figure 5) of tungsten and peroxide,[20] in which we plot potential referenced to a normal hydrogen electrode (NHE) versus pH. These curves are based on the Nernst equation:[24]

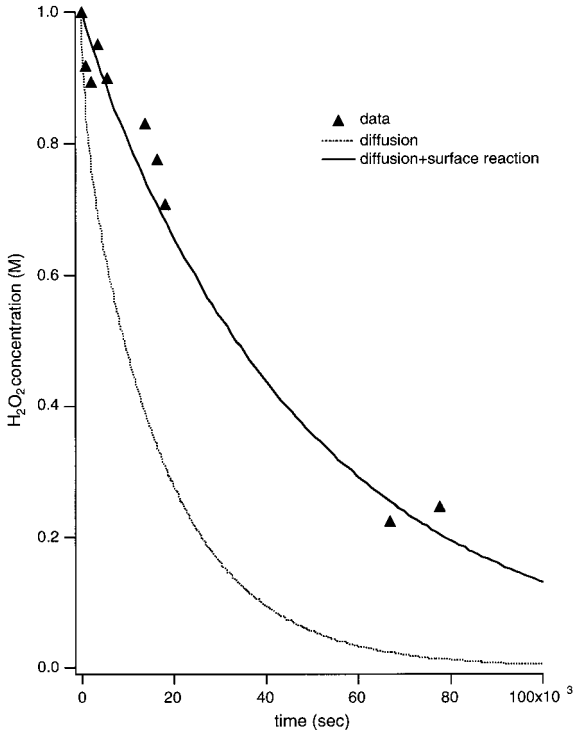

Figure 4. Comparison of the decay of H_2O_2 in a solution reacting with a W plate at one end with the theoretical time dependencies governed by diffusion and diffusion plus a chemical reaction at the metal surface, as given by the spatial averages of eqs 11 and 15, respectively.

$$E = E_0 + \frac{0.059}{n}\log\left[\frac{(A)^a}{(B)^b}\right] - 0.059\frac{m}{n}\text{pH} \qquad (4)$$

where E_0 is the static open circuit potential for the reaction at the electrode, (A) and (B) are the activities of the oxidized and reduced species, m is the number of H^+ ions, and n is the number of electrons needed to describe the oxidation of W and the reduction of peroxide. The diagram shows the regions of thermodynamic stability for the various tungsten oxides and for the two types of hydrogen peroxide. For example, in the bottom region of the diagram, only pure W is stable and is therefore immune to corrosion. At the upper left, WO_2, W_2O_5, and WO_3 occupy the regions as passive oxides at successively higher potentials in order of oxidation state. W_2O_5 is predicted to exist in only an extremely narrow range of potential and pH, which is why it is unlikely that the oxide formed upon etching the trioxide with H_2O_2[23] has that composition. On the other hand, WO_3 should dominate for all $E > 0.1$ V and pH < 4. This pH threshold is a consequence of our assuming an arbitrary concentration of the soluble ion WO_4^{2-}; the vertical line labeled "−6" represents the activity $(WO_4^{2-}) = 10^{-6}$. This ion should therefore appear in solution for the upper right portion of the diagram, which represents the conditions under which W is most likely to corrode. The vertical line on the right separates the stable region of H_2O_2 (pH < 11.6) from that of HO_2^- (pH > 11.6).

In our electrochemical experiment, we measured the potential and pH of the W plate and the peroxide solution, respectively, as a function of immersion time. Following some initial transients, V rapidly increased but leveled off within a few hours (Figure 6). Meanwhile, the pH steadily decreased (Figure 7). The plot of potential versus pH (Figure 8) superimposed on Figure 5 (solid circles) shows that the native oxide of W has a stoichiometry close to WO_3 and that this oxide remains stable

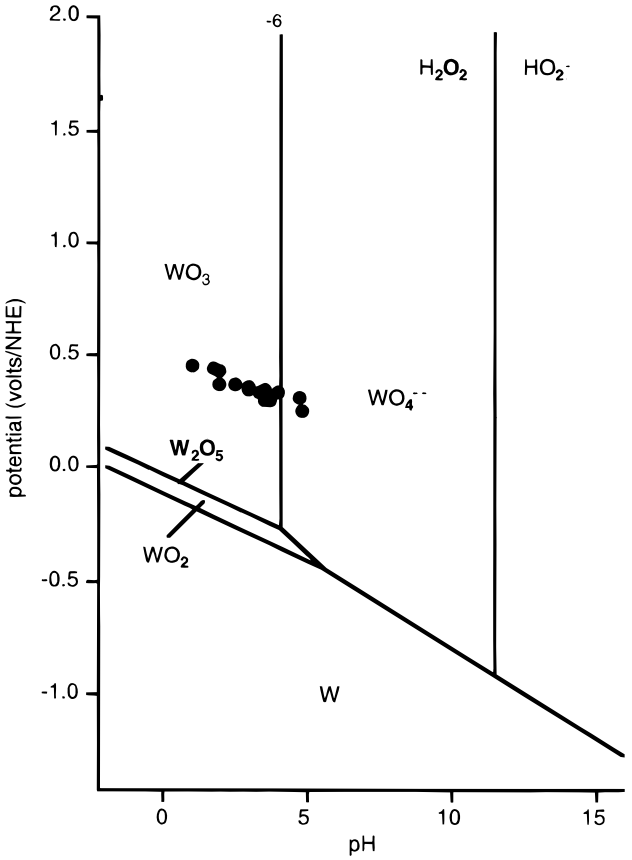

Figure 5. Pourbaix diagram of W and its oxides. The filled circles indicate the region of potential-pH in which the present measurements were performed.

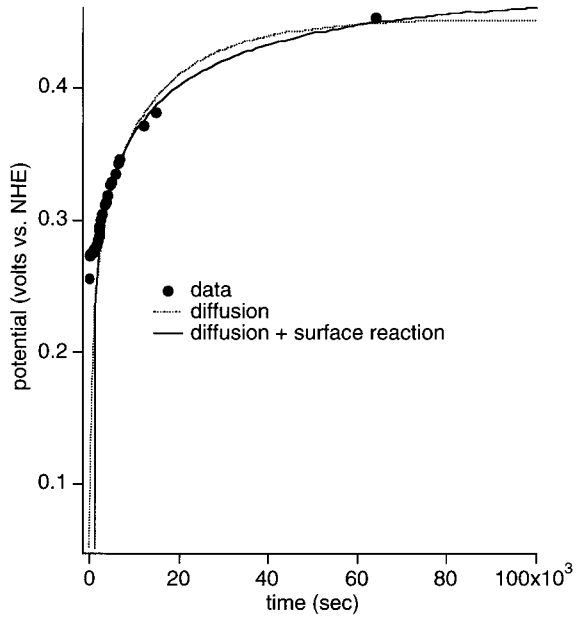

Figure 6. Open circuit potential of W versus time of immersion in 1 M H_2O_2 as compared to the Nernst equation incorporating the theoretical time dependence of the pH.

for the entire measurement. This is in agreement with the SERS data,[19] which show that the Raman bands of the oxide can be associated with a combination of anhydrous and hydrated forms of the trioxide and is also consistent with the similarity of the Raman spectrum of the dissolved oxide to that of the polytungstate (Figure 3). A fit of the data in Figure 8 gives

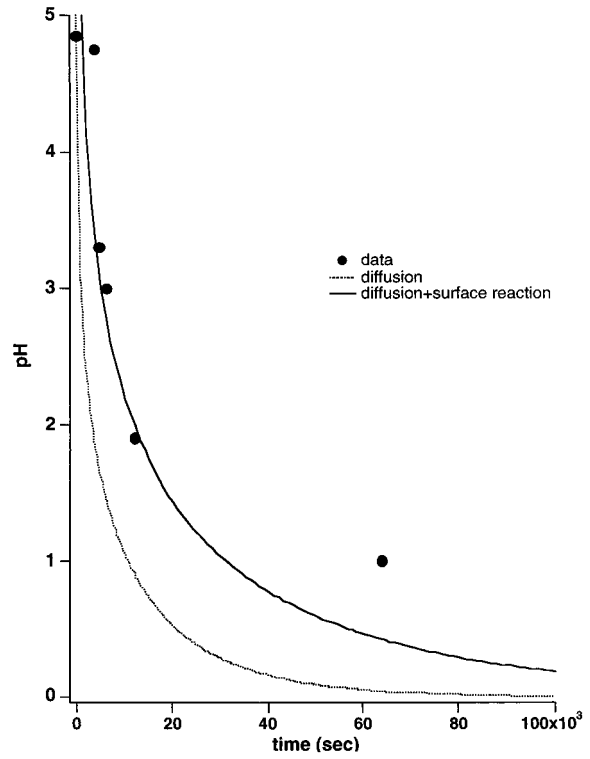

Figure 7. Time dependence of pH of the solution surrounding the W plate (circles). Dotted curve shows the theoretical time dependence based on the diffusion of H_2O_2 molecules to the interface. Solid curve accounts for diffusion plus a chemical reaction at this interface.

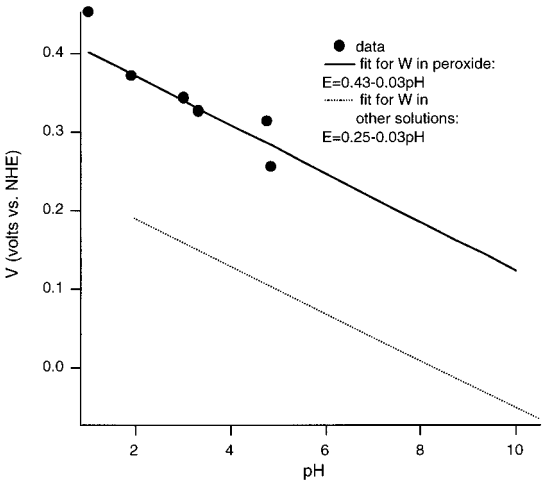

Figure 8. Open circuit potential versus pH of the W/H_2O_2 system for various immersion times (circles). Solid curve is a fit to the data. Dotted curve is a fit to data taken with three different buffer solutions (ref 25).

$$V = 0.43 - 0.03\,\mathrm{l}\qquad \mathrm{pH} \tag{5}$$

which has the same slope as the potential versus pH curve measured for W in three other buffer solutions[25] but is a factor of 2 too small to account for the simple oxidation of W to WO_2, W_2O_5, or WO_3 (Figure 5). A slope of 0.06 has been measured for W/W oxide electrodes in NaOH and H_2SO_4 at high temperatures, which is consistent with those oxidation processes.[26] From eq 4, a slope of 0.03 suggests that the set of reactions at the electrode involves twice as many electrons as H^+ ions. This implies that eq 1 cannot be the primary process governing the reaction at the interface; another positive ion may be involved to conserve charge.

The initial potential, with respect to NHE, was 0.34 at a pH

of about 4, indicating (Figure 5) that the stable oxide in air is WO_3. Upon immersion, the potential quickly (in about 0.5 h) dropped to 0.29, and the pH decreased to between 3.5 and 4.0; WO_3 is still stable in this regime. The potential then increased slowly while the pH continued to decrease. For instance, after about 10 h of immersion, the potential increased to 0.431 V, and the pH decreased to 2. This decrease in pH is consistent with the decomposition of peroxide (eq 3), which essentially reduces the amount of cathodic reactant.

Model of the Raman and Electrochemical Temporal Responses. In electrochemical measurements in which W was used as a rotating electrode in a H_2O_2 solution, it was found that the oxide dissolution rate was a function of the rotation speed,[23] signifying the importance of diffusion of H_2O_2 through the solution to the W surface. We can therefore model the time dependence of the concentration C of H_2O_2 molecules in the presence of W using the 1-D diffusion equation:

$$\frac{\partial C}{\partial t} = D\frac{\partial^2 C}{\partial x^2} \tag{6}$$

where $0 < x < L$ is the distance from the W surface ($x = O$), and D is the diffusion coefficient of H_2O_2. Equation 6 is subject to the initial condition

$$C(x > 0, t = 0) = C_0 \tag{7}$$

which corresponds to a uniform concentration of H_2O_2 prior to immersion of W, and the boundary conditions

$$C(x = 0,t) = 0 \tag{8}$$

and

$$\frac{\partial C}{\partial x} = 0 \text{ at } x = \mathrm{L} \tag{9}$$

In eq 8, we assume that each H_2O_2 molecule is annihilated instantaneously at the W surface. Equation 9 corresponds to the fact that there is no flux of H_2O_2 across the cell wall, which is impermeable. The Laplace transform of eq 6 with the above constraints is

$$\bar{C}(x,p) = \frac{C_0}{p}\{1 - \sum_{n=0}^{\infty}(-1)^n[\mathrm{e}^{-q(2L(n+1)-x)} + \mathrm{e}^{-q(2nL+x)}]\} \tag{10}$$

where p is the Laplace transform operator, and $q^2 = p/D$. The inverse transform of eq 8 is

$$C(x,t) = C_0\left\{1 - \sum_{n=0}^{\infty}(-1)^n\left[\mathrm{erfc}\left(\frac{2L(n+1)-x}{2\sqrt{Dt}}\right) + \mathrm{erfc}\left(\frac{2nL+x}{2\sqrt{Dt}}\right)\right]\right\} \tag{11}$$

where erfc is the complementary error function, and we have used the relation

$$\frac{1}{(1+\mathrm{e}^{-\Phi})} = \sum_{n=0}^{\infty}(-1)^n\mathrm{e}^{-n\Phi} \tag{12}$$

as derived from the binomial expansion to obtain eq 10.

In the Raman experiment, the incident laser beam, which traverses the entire length of the cell, is directed perpendicular to the W plate. In order to compare the result of the diffusion calculation to the data, we numerically averaged eq 11 over the length of the cell for fixed times up to 10^5 s. This was roughly twice the characteristic diffusion time (L^2/D) across the cell. Figure 4 shows the time dependence of the spatial average of eq 11 for $D = 2.2 \times 10^{-5}$ cm^2/s[27] in comparison to the experimentally measured $C(t)$. Clearly, the measured concentration of H_2O_2 decreases much more slowly than predicted by the theory. Part of this discrepancy results from the fact that the actual area of the W plate exposed to the bulk solution is smaller (by a factor of roughly 0.75) than the cross-sectional area of the solution perpendicular to the plate. However, we surmise that the main cause of disagreement is our assumption of instantaneous absorption at the interface. Presumably, some of the H_2O_2 molecules will be reflected back into the solution upon arriving at the interface. One reason for this may be that each site on the $x = 0$ plane can be occupied by only one molecule. A vacancy is established only after the molecule reacts with the W surface, leaving room for another molecule to become adsorbed and react.

In order to more realistically describe the diffusion process, we account for a finite heterogeneous reaction rate constant k (in cm/s) with the W surface. The mathematics is simplified by taking the W surface to be at $x = L$. Now we have zero flux at $x = 0$, and the boundary condition at $x = L$ becomes

$$-D\frac{\partial C}{\partial x} = kC \tag{13}$$

This situation is analogous to 1-D heat flow with zero flux at $x = 0$ and radiation at $x = \mathrm{L}$.[28] The Laplace transform of eq 6 for the new boundary conditions is

$$\bar{C}(x, p) = \frac{C_0}{p}\left\{1 - \frac{k\cosh qx}{qD\sinh qL + k\cosh qL}\right\} \tag{14}$$

The solution, via the Laplace transform integral, is

$$C(x,t) = 2kC_0\sum_{n=1}^{\infty}\frac{\exp(-\alpha_n^2 Dt)\cos\alpha_n x}{\left[k + \left(\frac{k^2}{D} + \alpha_n^2 D\right)L\right]\cos\alpha_n L} \tag{15}$$

where α_n is the root of the equation

$$\alpha L\tan(\alpha L) = kL/D \tag{16}$$

Equation 15 is numerically averaged over the length of the cell and then plotted in Figure 4. For $k = 3 \times 10^{-5}$ cm/s, the agreement with the data is much better than in the case of diffusion without a surface reaction. Values of $k > 1 \times 10^{-3}$ cm/s give a result that is almost indistinguishable from the case of instantaneous absorption. Recently, the surface reaction rate for the bleaching of WO_3 films by H_2O_2 was derived by assuming that eq 1 governs the reaction at the interface and numerically solving the diffusion equation for the motions of the electron and H^+ through the oxide film.[29] A fit of the decay of the absorbance yielded the rate 7×10^{-5} (cm/s) (M^{-1}) or 7×10^{-5} cm/s for 1 M H_2O_2, close to what we determined from our Raman data. It was concluded that the rate-limiting step in decoloration of films by H_2O_2 was not the diffusion of H_2O_2 to the W surface, nor that of H^+ within the oxide film, but was a (charge transfer) reaction at the oxide surface, in agreement with our analysis of the kinetics of the peroxide decay.

The simple boundary conditions that we have considered do not explicitly account for the separate steps typically involved in catalytic reactions:[30] trapping in a mobile precursor state,

adsorption of peroxide, desorption, lateral interactions between oxide molecules, or diffusion through the oxide to the bare metal. We also do not know whether these reactions are governed by first- or second-order kinetics. This information could be obtained by separate measurements of the concentration dependence of the reaction rates. Additionally, we do not account for dependence of the reaction rate on the surface coverage of the adsorbed molecules. The value of k that we have obtained is therefore an effective rate constant that encompasses all of these different processes.

In order to model the time dependence of the open circuit potential (Figure 6), we assume that, since the kinetics are slow, the system remains close to thermal equilibrium, enabling us to employ a time-dependent Nernst equation. Therefore, we allow several of the parameters in eq 4 to have a time dependence: $E = E(t)$, $(A) = (A(t))$, $(B) = (B(t))$, and $\mathrm{pH} = \mathrm{pH}(t)$. It is difficult to write an explicit expression for the second term in eq 5 without knowing precisely the set of reactions at the W/H_2O_2 interface that give rise to the parameters of eq 5. However, the time dependence of E may actually be dominated by the third term in eq 4. This would reflect equal rates of oxidation and reduction in equilibrium. In fact, when we subtract the measured $\mathrm{pH}(t)$ (times a constant) from the measured $E(t)$, we obtain a function that is approximately independent of time. In theory, if we consider that the source of H^+ ions is the dissociated H_2O_2 (eq 3), then the time dependence of the pH can be determined by eq 3 and the number of H_2O_2 molecules that decay from eqs 11 or 15. Consequently, we have

$$[H^+](t) = C_0 - C(t) \tag{17}$$

In Figure 7, we plot $\mathrm{pH}(t) = -s \log\{[H^+](t)\}$ (s is a scale factor to account for the initial pH of the solution). We expect this function to decay more rapidly than the measured $\mathrm{pH}(t)$ since the H^+ ions are presumably generated only at the W surface ($x = 0$), not throughout the solution, as eq 17 would suggest. Additionally, as was explained above to account for the discrepancy between theory and measurement in Figure 4, the finite probability of reflection of H_2O_2 molecules at $x = 0$ delays their dissociation into H^+ ions. Again, the latter seems to be the primary cause of disagreement between the data and the theory based solely on diffusion. As shown in Figure 7, when we account for the finite reaction rate at the W surface, we see that the agreement is reasonably good.

When $\mathrm{pH}(t)$ is substituted into eq 4, with the second term and slope of pH treated as fitting parameters, we obtain the curve shown in Figure 6. The agreement with the data is surprisingly good, for long times, for both types of boundary conditions. However, for short times, the system is too far from equilibrium to allow eq 4 to appropriately describe the dynamics of the open circuit potential.

Conclusions

The interaction between the long-lived radiolysis product hydrogen peroxide and tungsten was studied by Raman spectroscopy and electrochemical techniques. Both methods showed that the native oxide of tungsten is hydrated, with a stoichiometry close to the trioxide, in agreement with our previous surface-enhanced Raman measurements. The main effect of the peroxide is to increase the solubility of the tungsten trioxide rather than to change the tungsten oxidation state. Therefore, as a function of immersion time, the peroxide Raman signal decays, while the signals associated with the dissolved tungsten trioxide increase. However, the reaction involves the decomposition of the peroxide into its ion, even though the latter is unstable at the low pH of the solution. The presence of this ion plus that of the tungsten oxide hydrates shows that the stability diagram of potential versus pH needs to be reexamined for both peroxide and tungsten, particularly at low pH. Meanwhile, the complete set of equations governing the interfacial reactions between these substances is still unknown.

The slow kinetics of the decay of the peroxide concentration was modeled by considering the 1-D diffusion of the peroxide molecules to the W surface, followed by a surface reaction represented by a single parameter k. This model provided a good account of the time dependence of the peroxide concentration, the pH, and the W open circuit potential. Our Raman results are consistent with electrochromic measurements of the same system. However, the electrochemical data indicate that there may be more reactions involved than the standard one (eq 1) used to describe the electrochromic process. In particular, we have seen evidence that another positive ion, besides H^+, is involved. For example, it has been speculated that H^+ is more rapidly transported through hydrated tungsten oxide films in the coloration reaction by converting it into H_3O^+ as it migrates between neighboring water molecules.[11] The latter ion plus the peroxide ion can also be produced via the decomposition pathway

$$H_2O_2 + H_2O = HO_2^- + H_3O^+$$

We believe the present work demonstrates the utility of combining normal Raman spectroscopy with simple electrochemical measurements as in-situ probes of reactions at liquid−solid interfaces. When the reaction kinetics are slow, we find that the Raman signal associated with the oxidizing species can be correlated with the electrochemical parameters by invoking a time dependence in the Nernst equation. This approach would certainly not apply to the nonequilibrium situation associated with the interaction of short-lived radiolysis products (HO_2 and OH, for instance) with metal surfaces, but we hope to explore this regime using ultrafast optical techniques.

Acknowledgment. We thank Laurie S. Waters and Walt F. Sommer, Jr., project leaders of the materials science portion of the Accelerator Production of Tritium (APT) program at the Los Alamos National Laboratory, for directing this research and for funding and Luke L. Daemen, R. Scott Lillard, and Andrew P. Shreve for useful discussions.

References and Notes

(1) Aveston, J. *Inorg. Chem.* **1964**, *3*, 981.
(2) Griffith, W. P.; Lesniak, P. J. B. *J. Chem. Soc. A* **1969**, 1066.
(3) (a) Gonzalez-Vilchez, F.; Griffith, W. P. *J. Chem. Soc. Dalton Trans.* **1972**, 1416. (b) Weinstock, N.; Schulze, H.; Müller, A. *J. Chem. Phys.* **1973**, *59*, 5063.
(4) Salje, E. *Acta Crystallogr. A* **1975**, *31*, 360.
(5) Daniel, M. F.; et al. *J. Solid State Chem.* **1987**, *67*, 235.
(6) Aubry, C.; et al. *Inorg. Chem.* 1**991** 3*0*, *4*409.
(7) Kim, D.; et al. *Catal. Lett.* **1995**, *33*, 209.
(8) Shiyanovskaya, I.; et al. *J. Mol. Struct.* **1995**, *348*, 99.
(9) Hardcastle, F. D.; Wachs, I. E. *J. Raman Spectrosc.* **1995**, *26*, 397.
(10) Wadayama, T.; Wako, H.; Hatta, A. *Mater. Trans., JIM* **1996**, *37*, 1486.
(11) Reichman, B.; Bard, A. J. *J. Electrochem. Soc.* **1979**, *126*, 583.
(12) Faughnan, B. W.; Crandall, P. S.; Heyman, P. M. *RCA Rev.* **1975**, *36*, 177.
(13) Deb, S. K. *Philos. Mag.* **1975**, *27*, 801.
(14) Schrimer, O. F.; Wittwer, V.; Baur, B.; Brandt, G. *J. Electrochem. Soc.* **1977**, *124*, 749.
(15) Russell, G. J.; Pitcher, E. J.; Daemen, L. L. *AIP Conference Proceedings 346, International Conference on Accelerator-Driven Trans-*

mutation Technologies and Applications, Las Vegas, NV, 1994; Arthuer, E. D., Rodriguez, A., Schriber, S. O., Eds.; American Institute of Physics: New York, 1995.

(16) Magee, J. L.; Chatterjee, A. In *Kinetics of Nonhomogeneous Processes*; Freeman, G. R., Ed.; John Wiley & Sons: New York, 1981; p 171.

(17) Byalobzheskii, A. V. *Radiation Corrosion*; Israel Program for Scientific Translations, IPST Cat. No. 5655; 1970.

(18) van den Meerakker, J. E. A. M.; Scholten, M.; van Oekel, J. *J. Thin Solid Films* **1992**, *208*, 237.

(19) Lillard, R. S.; Kanner, G. S.; Butt, D. P. *J. Electrochem. Soc.* In press.

(20) Pourbaix, M. *Atlas of Electrochemical Equilibria in Aqueous Solutions*; National Association of Corrosion Engineers: Houston, TX, 1974; p 280.

(21) Soptrajanov, B.; Nikolovski, A.; Petrov, I. *Spectrochim. Acta* **1968**, *24A*, 1617.

(22) Pelletier, M. J.; Davis, K. L.; Carpio, R. A. *Electrochemical Society Proceedings*; Reno, NV, 1995.

(23) van den Meerakker, J. E. A. M.; Scholten, M.; van Oekel, J. J. *J. Electroanal. Chem.* **1992**, *333*, 205.

(24) Jones, D. A. *Principles and Prevention of Corrosion*; Macmillan Publishing Co.: New York, 1992.

(25) Lillard, R. S.; et al. Los Alamos National Laboratory Internal Report LA-UR-97-116.

(26) Kriksunov, L. B.; Macdonald, D. D.; Millet, P. J. *J. Electrochem. Soc.* **1994**, *141*, 3002.

(27) Pimblott, S. M.; LaVerne, J. A. *J. Phys. Chem.* **1994**, *98*, 6136.

(28) Carslaw, H. S.; Jaeger, J. C. *Conduction of Heat in Solids*; Oxford University Press: London, 1959; p 315.

(29) Kikuchi, E.; et al. *J. Electroanal. Chem.* **1995**, *381*, 15.

(30) van Santen, R.A.; Niemantsverdriet, J.W. *Chemical Kinetics and Catalysis*; Plenum Press: New York, 1995.